UNIVERSITY OF CALIFORNIA, SAN DIEGO

Human electrocortical dynamics of unrestricted upright gait and spatial navigation in a square spiral track

A thesis submitted in partial satisfaction of the

requirements for the degree of Master of Science

in

Biology

by

Jason Daniel Trees

Committee in charge:

Terrence Sejnowski, Chair
Eric Halgren
Eduardo Macagno
Howard Poizner

2015

The thesis of Jason Daniel Trees is approved, and it is acceptable in quality and form for publication on microfilm and electronically:

_____

_____

_____

_____

Chair

University of California, San Diego

2015

DEDICATION

I dedicate this thesis to my loving wife, Kayla. Without her strength and support, none of this would have been possible. And to my two children, Jaron and Elladyn, who will always serve as my inspiration and joy.

EPIGRAPH

"I am trying to wake your sleeping mind to the subtle language the world is whispering. I am trying to seduce you into understanding."

- Patrick Rothfuss, The Wise Man's Fear

TABLE OF CONTENTS

LIST OF FIGURES

LIST OF TABLES

ACKNOWLEDGEMENTS

I would like to express my gratitude to my supervisor Howard Poizner for all of the useful comments, critiques, and encouragement. I have learned more than I could have imagined from my time in the Poizner Lab. In addition, I would like to thank Joseph Snider for introducing me to this topic and many others, and bearing with my many questions. I would like to thank the chair of my thesis committee Terrence Sejnowski and the other members, Eric Halgren, Eduardo Macagno, and Howard Poizner for giving me this opportunity to share the culmination of my work. Lastly, I would like to thank my loved ones, who have encouraged me throughout this process.

ABSTRACT OF THE THESIS

Human electrocortical dynamics of unrestricted upright gait
and spatial navigation in a square spiral track

by

Jason Daniel Trees

Master of Science in Biology
University of California, San Diego, 2015
Professor Terrence Sejnowski, Chair

The study of human locomotion and spatial navigation in a naturalistic paradigm is vastly understudied. It has recently been shown that electrocortical activity is coupled to steady-speed human gait. Previous work has also shown a relation between delta/theta-band (2-8 Hz) activity over parietal cortex and a subject's spatial location. Our aim was to determine if the same electrocortical findings in steady-speed walking were present in unrestricted, self-initiated ambulation, and if

similar spatial context related neural signals could be found in a different spatial task. We simultaneously recorded electroencephalography (EEG) and full body motion of twelve young healthy subjects walking at two self-directed speeds, slow and brisk, through a 4x4m square spiral track. The EEG data were filtered and cleaned using semi-automated means and infomax Independent Component Analysis (ICA), allowing for removal of muscular, ocular, and other artifactual signals. Gait normalized Event Related Spectral Perturbations (ERSP) were obtained, showing significant cyclical intra-stride changes in power of the delta/theta-band (3-8 Hz) in the 'slow' speed condition, and alpha/beta-band (9-25 Hz) in the 'brisk' condition only. Significant delta/theta-band decreases in power were also observed near the center point of the swing phase of each leg in the 'brisk' condition. Additionally, the data from parietal electrodes were filtered from 2-8 Hz, the analytic amplitudes were calculated and co-localized to the subject's position in space. Analysis of these data over each segment of the spiral showed significant activity in the same relative spatial location across segments. Further examination using these techniques could lead to a better understanding of diseases with motor and spatial navigation deficits, like Parkinson's and Alzheimer's disease.

INTRODUCTION

The study of neuroscience is one of the fastest growing fields, with widespread impact on many areas such as medicine, biology, computer science, and engineering. Understanding how our brains work allows us to better understand how we interact with our bodies, environment, and other people. Though it would be more straightforward to do all of this research directly on humans, ethical, legal, and logistical restrictions limit the type and methods of research that can be done on humans. Given these restrictions, many turn to animal models with the ultimate goal of bringing understanding to processes, like spatial navigation (Wills et al., 2013; Buzsaki and Moser, 2013; Aronov and Tank, 2014; geva-Sagiv et al., 2015), memory (Leutgeb and Mizumori, 1999; Buzsaki and Moser, 2013; Vorhees and Williams, 2014), and motor control (Petersen, 2014) that are shared with humans in an effort to better understand our own brains. In order to do direct research on humans, these common roadblocks in neural research must be overcome. One of the largest hurdles is how to get access to data from the brain in a non-invasive way. The two primary non-invasive methods to obtain neural data are functional Magnetic Resonance Imaging (fMRI) and electroencephalography (EEG). fMRI measures the blood-oxygen-level dependent (BOLD) signal, an analogue for the change in metabolic activity of region specific neurons, whereas EEG records the direct electrical field produced by neural activity. The advantage of fMRI is a high spatial resolution in recordings, but the tradeoff is the temporal accuracy as a result (Recording frequency: ~ 0.5Hz). EEG has the opposite advantage, trading low spatial resolution for high

temporal resolution (Recording frequency: ~1000Hz). In addition to the restrictions of the data produced, fMRI constrains the subjects to be completely prone within the scanner and maintain an absolutely stationary head. EEG, on the other hand, provides less physical constraints and can be portable, allowing subjects to physically move freely through an environment while data are recorded.

Due to the inherent restrictions and limitations of recording human subjects, there is a startling lack of empirical human neuroscience studies on topics that are relatively "well studied." One of these areas is the neural correlates of unrestricted walking and gait. Most gait literature is traditionally neurobehavioral or biophysical (Cimolin and Galli, 2014; Hsu et al., 2014). In addition, many gait related studies eschew the basic understanding and jump straight to disease related abnormalities in gait, such as Parkinson's disease (Delva et al., 2014). While these are valid topics of research, a more basic understanding of the neural correlates of gait in a naturalistic environment should be addressed.

There have been attempts at understanding the brain and gait in humans, but are restricted to steady-speed treadmill walking or gait-assisted leg movements. These studies ultimately fail to create a naturalistic environment and paradigm that mirrors the way in which humans ambulate on a day to day basis. Seeber and colleagues (2014) demonstrated that there is beta (18-30 Hz) frequency suppression over sensorimotor areas during upright walking when compared to simple upright standing. In addition, during the actual walking times, they saw low gamma (24-40 Hz) frequency had periods of suppression and activation that coincided cyclically with the gait cycle. One key feature to note is that this experiment was conducted on

young, healthy adults in a robotic gait orthosis (Lokomat, Hocoma, Switzerland), used mainly for physical rehabilitation. In addition, the robot was operated at 100% guidance force. This essentially forced the subjects' legs into a gait-like movement pattern, while not actually having the subjects ambulate. While the sensorimotor feedback in this situation might be somewhat similar to actual walking, there is no initiation or control of movement on the subjects' part, simply an entrainment to the rhythm of the robot orthosis's movement.

Similarly, Gwin et al. (2010) aimed to elucidate the spectral properties of EEG tied to the gait cycle. In this case, Gwin and colleagues had subjects walk at a steady speed on a treadmill while recording the neural electrical activity from EEG. Through source localization of ICA cleaned EEG data, they found sources with significant changes in spectral power in the anterior cingulate, posterior parietal, and sensorimotor cortex areas. Their findings included alpha- and beta-band power increases in both sensorimotor cortices and the frontally located, anterior cingulate area. In addition, they showed evidence of lateralization of signal between the sensorimotor cortices, with a more pronounced increase in power for the contralateral limb "push-off" event. These results were obtained from subjects moving their own legs at a steady speed on a treadmill. This represents a significant step towards studying natural human ambulation, but the underlying task remains to align the gate with an external reference, the treadmill in this case. On a treadmill, the gate related characteristics of motion are altered by the lack of natural gate speed modulation and subjects not actually propelling themselves.

Taking a further step back from an upright walking paradigm and to increase the quality of EEG signal by restricting what is seen as auxiliary motor activity, experiments were conducted to limit the subjects to sitting still and moving only discrete limbs or none all (Heideman et al., 2014). Electrocortical signals show modulation of specific frequency bands to movement of the lower limbs after entraining to experimental cues. Like the previous experiments mentioned, beta-band power changes in response to a regular stimulus and movement. The rhythmicity of the effect has been implicated in motor movements such as human gait. Analysis of gait even extends into the analysis of humans observing others walking, eschewing any embodied motor movement recording. Like the experiments before, the authors show significant spectral power changes in the EEG, though this is in response to observing gait in different orientations (normal, upside-down). The findings do not attempt to demonstrate the neural signals of actually walking, but show a significant neural involvement in at least the perception of walking.

Spatial navigation is another area that is well studied in animals (Wills et al., 2013; Buzsaki and Moser, 2013; Aronov and Tank, 2014), but severely understudied in humans. Spatial navigation is the process by which an animal receives input from its environment, processes the information, and then behaviorally navigates the physical space in response to that specific information.

In order to function effectively in complex environments, mammals have developed unique brain structures and neural circuits to process external spatial information, such as the hippocampus (HC) and entorhinal cortex (EC) of the medial temporal lobe (Bush et al., 2014; Cabro et al., 2014), along with the parietal cortex

(Nitz, 2012; Svoboda et al., 2015). It has been extensively shown in rats that the HC and EC, along with surrounding regions, are active and necessary for such animals to conduct a spatial navigation task (Derdikman and Moser, 2010; Wills et al., 2013; Buzsaki and Moser, 2013; Aronov and Tank, 2014; geva-Sagiv et al., 2015)). To a lesser degree, this has also been shown in non-human primates (Etienne et al., 2014; Furuya et al., 2014), other non-human mammals (Geva-Sagiv et al., 2015), and humans (Lithfous et al., 2013; Watrous et al., 2013).

The vast majority of data available on spatial navigation comes from experiments conducted on rats (*Rattus norvegicus*). Though rats and humans are different species, the overall neural architecture, circuitry, and biochemistry of their brains are similar. The advantage of conducting experiments on rats is that you can obtain single unit recordings, from surgically implanted electrodes innervating the brain region of interest that can be processed to show an individual neuron's action potential firing profile. There are two main systems, located primarily in the hippocampus (HC) and entorhinal cortex (EC) of the MTL, that have been found to be involved in the processing of the spatial environment. The first neuronal type tied to spatial location of the rat was the so-called "place cell" (O'keefe, 1976). Neurons recorded from the Cornu Ammonis 1 (CA1) region of the HC showed increased activity when the animal traversed a specific location in its environment while freely exploring. The "place" at which these individual neurons fire is locked to the external environment, and a single neuron can have differential activation in different environments (Muller and Kubie, 1987). The firing pattern of these cells provided the

first neural basis for the perception of allocentric location, which is the perception of where one is, within an environment with an external reference frame.

Another major spatially relevant neuronal type was recently discovered and named "grid cells," because they responded in a tessellated triangle grid-like pattern, with a single neuron spiking at the intersection points of every triangle in the grid. The Moser group (Edvard Moser and May-Britt Moser) found these fascinating neurons in the EC (Hafting et al., 2005). Each of the cells can fire in different grid-phase (the offset of the nodes in respect to an external x and y axes), orientation (the angle nodes successive nodes follow when compared to the external axes), and size (relative size of each node compared to the external environment). All of this results in the population of grid cells fully covering a given environment. From these cells, the start of a two-dimensional representation of the environment emerges. It has been recently theorized that the summation of grid cell activity that overlaps at any given spot, can lead to the formation of a corresponding place cell (Fyhn et al. 2007). A unique feature of both place and grid cells is that the rat has to be actively moving and navigating the environment to illicit activity (Richard et al., 2013). The brain takes multimodal sensory input to create an accurate representation of the external environment. In order for the most accurate "spatial maps" to be created, self-motion signals, including vestibular (balance and acceleration), proprioceptive (position of limbs in space relative to the rest of the body), and visual streams, among others, are essential (Terrazas et al. 2005; McNaughton et al., 2006).

While the hippocampus and related structures have been the primary regions implicated in spatial processing and navigation, other cortical areas, like the parietal

cortex, have been shown to have a function in spatial processing (Anderson, 1995). In addition, individual cells in the rat parietal cortices respond to spatial features in the environment, similar to those found in the HC (Nitz, 2006; Nitz 2012). Another type of cell, labeled "route cells", respond to specific features of a spatial route in a scalable manner, irrespective of spatial location and direction (Nitz 2012). It is known that there are extensive connections between the HC and parietal cortex, and as such, it is reasonable to conclude some processing and communication of mutual information (Clower et al., 2001). Cortical processing of spatial information, specifically in parietal regions within rat models leads to the possibility of similar processing in those regions in larger mammals, like humans.

To help understand the details of spatial navigation in humans in realistic environments, an area where little is known, the Poizner lab has pioneered the study of freely moving human subjects in spatial navigation and memory experiments using EEG. An EEG signal is a time series, and as such, can be broken down into its component frequencies. It is common practice within the field to use standardized frequency ranges for time series and spectral power analysis. Within the high delta/theta frequency band (2-8Hz), recorded from midline parietal electrodes, the EEG signal not only has a relation of power to speed similar to findings in rats, but also contains information for spatial maps (Snider et al., 2013). Theta-band activity in rat hippocampus and entorhinal cortex has been shown to be important for processing of place and grid cell activity, and communication of that activity to other brain regions (Burgess and O'Keefe, 2011). In addition, quantification of these maps has shown a positive correlation of strength between spatial maps of parietal theta activity

with unsupervised learning of objects within an environment (Snider et al., 2013). In a separate experiment, initial results show a modulation of low frequency (2-5 Hz) power over central parietal electrodes locked to traversal of segments of a square spiral, regardless of segment length, orientation, or subject direction (Trees et al., 2013). These results indicate large involvement of cortical regions in gait and spatial navigation and warrant further study.

There is no previously published experiment, which we are aware of, in which human subjects are able to freely move about physical space while recording full body position and scalp EEG. To address this gap in understanding, we designed an experiment in which subjects walk through a 4x4 meter square spiral track while recording EEG and full body motion capture simultaneously. Subjects were instructed to walk at 'slow' and 'brisk' speeds in two separate conditions. From the limited published literature on gait related EEG, most notably from steady speed treadmill walking, we hypothesize that spectral characteristics of the EEG will show cyclical changes in power associated with the normalized gait cycle. Specifically, intra-stride changes of power in the alpha-/beta-bands (~9-25 Hz) mainly happening within the swing phase of each leg, along with changes in theta-band (4-8 Hz) power, should decrease during the swing and increase during the stance phases where both legs are in contact with the floor. In addition, from the gait orthosis assisted lower leg movement study, high beta/ low gamma-band (25-40 Hz) power also has been shown to change cyclically with the gait cycle. As far as spatial related analysis of freely moving humans in a physical environment, to our knowledge there is only the previous work done within our own lab. From that work, we hypothesize that we will see EEG signal

from parietal electrodes being associated in some way with the subjects' navigation and location. Additionally, preliminary results show a low frequency (2-5 Hz) modulation of the analytic amplitude from the midline parietal electrode (Pz) being locked to the traversal of each spatial segment of the spiral (Trees et al., 2013). As such, we aim to see if similar frequency specific activity occurs across each of the spatial segments of the spiral.

MATERIALS AND METHODS

Subjects

Twelve right-handed human subjects participated in the study. The average subject age was 24.8 +/- 4.4 (mean +/- standard deviation) years. Seven of the subjects were male and five were female. They all had normal or corrected to normal vision (with contacts), and no history of neurological or psychological disorders. All metal was removed from each subject's face and head area. Written, informed consent was obtained from all subjects, and the experiments were approved by the University of California, San Diego Institutional Review Board.

Experimental Setup

A straight-edged square spiral pattern, with an outermost edge length of four meters, was taped out on the lab space floor (Figure 1a) The edges of each turn became progressively smaller by 0.5 meters (the width of the track) as it spiraled inwards. Subjects wore a full body motion-tracking suit with thirty infrared markers placed as described below (PhaseSpace Inc.). In addition, they were required to wear a backpack to carry the EEG amplifier and battery. A thin flexible fiber optic cable connected the amplifier, up through the roof, to the recording computer, allowing for maximum freedom of movement. The experiment itself was programmed using the Vizard 4.0 virtual environment software (WorldViz, Inc.). 64 channel, high-density EEG (Biosemi ActiveTwo, Biosemi Inc.) data were recorded during the entire experiment. Simultaneously, kinematic data from the motion tracking suit were

recorded. Data streams were synchronized to a timing pulse after the experiment for analysis (Snider et al., 2013).

Walking Task

Subjects were instructed to walk in between the taped out spiral boundaries, starting at the outermost segment. They were tasked with walking in towards the center of the spiral, and once reaching the center, turning around and walking back out. Reaching the start of the spiral, they again turned around and headed back towards the center, repeating this for a total time of ten minutes (Figure 1A). The experiment was broken up into two speed conditions, "slow" and "brisk". During the "slow" condition, each subject was instructed to walk at a "slow, leisurely pace, like you are not in a hurry to get anywhere." In the "brisk" condition, they were instructed to walk at a "quicker, brisk pace, like you are late to class, but not to run or jog." Each subject walked at their own self-directed speed for each condition. No threshold physical speed was enforced, though subjects were monitored to make sure they were complying with the instructions. The speed condition was counterbalanced across the subject population.

Data Collection

Motion capture

Kinematic data were recorded using the Phasespace (Inc.) Impulse X2 motion capture system. Twenty-four optoelectronic cameras were arrayed around the lab to give full coverage of the square spiral space. Thirty active infrared light emitting diodes (IRLEDs) were placed around the subject's suit to capture the full body

kinematics during the experiment. Each leg had three markers placed on the foot, one on the knee, and one on the front hip. Each arm had three markers placed on the hand, one on the elbow, and one on the shoulder. Markers were placed at the center of the chest and stomach, the center of the back between the scapulae, and one each to the left and right of the lower back. Lastly, five markers were placed on the head in a diamond orientation, with one of the points centered on the forehead. The IRLEDs were driven by the motion capture system's controller, connecting wirelessly with the accompanying server. The data were recorded at 120 Hz. The motion capture system was previously shown to have an accuracy of about 1mm throughout the room (Snider et al., 2013)

EEG data

Electrocortical data were recorded using a Biosemi high-density EEG electrode array with 64 scalp electrodes and 8 external electromyogram (EMG) electrodes. Each electrode was individually preamplified at the recording site before the signal was sent to the EEG amplifier. Four of the EMG electrodes were used as electrooculogram (EOG) channels, placed above and below the right eye, as well as lateral to the right and left eye. Another two of the external electrodes were placed on the back of the left and right neck, at the height of the 7th cervical vertebra. These electrodes were used to monitor the activity of the neck muscles, particularly the trapezius. The last two EMG electrodes were placed behind the ears on the mastoid bones. These were used as the reference for the scalp electrodes. Electrode locations

were digitized in 3D space with the Fastrak system (Polhemus Inc.) in combination with the Locator software suite (SourceSignalImaging Inc.).

Data Processing and Analysis

Gait - Kinematics

The raw motion capture data from the toe and heel markers of each foot was used to extract gait related events. Using Python 2.7 (www.python.org), we developed a program to manualy assign the location of the gait events into the motion capture data framework. The vertical displacements for the toe and heel markers were displayed in individual plots. Using manual visual inspection, the lift events and contact events for each of the markers were recorded by selecting the appropriate point from the kinematic marker trace. The foot kinematics were rather regular and proved to be easily distinguished by eye (Figure 2). A three-dimensional recreation of all the foot markers that scrolled with the data was used to confirm the appropriate kinematic behavior with each event.

Gait - EEG

Signal processing of the EEG for the gait based analysis was done mainly using the EEGLAB toolbox (Delorme and Makeig, 2004) for Matlab (MathWorks Inc.). The data were baselined to the average of the two mastoid electrodes, high pass filtered above 1 Hz, and low pass filtered below 55 Hz. The relevant gait events were read into the EEG data structure. The data were then epoched from the start of each gait cycle to the size of the maximum gait cycle per subject. Epochs containing artifacts were rejected based on the automated algorithms built in to EEGLAB and

through manual visual inspection. Independent component analysis (ICA) was conducted on the resulting epochs (Bell and Sejnowski, 1996). Independent components (ICs) containing ocular, muscular, and other artifactual signals were removed. An average of 8.7 +/- 3.8 (mean +/- standard deviation) ICs were kept per each subject. The data were re-epoched to the same starting event but with an additional 1000 ms before and after the original epoch dimensions to allow for event related spectral analysis in the low frequency range (3+ Hz). The remaining ICs were used to backproject the "cleaned" data to the original electrode space. The final electrode signals were averaged to twelve anatomically relevant clusters for condensed analysis. Those are left frontal (AF3, F1, F3, F5), midline frontal (AFz, Fz), right frontal (AF4, F2, F4, F6), left sensorimotor (FC1, FC3, FC5, C1, C3, C5), midline sensorimotor (FCz, Cz), right sensorimotor (FC2, FC4, FC6, C2, C4, C6), left parietal (CP1, CP3, CP5, P1, P3, P5), midline parietal (CPz, Pz), right parietal (CP2, CP4, CP6, P2, P4, P6), left occipital (PO3, PO7, O1), midline occipital (POz, Oz), and right occipital (PO4, PO8, O2).

The resulting data clusters were used in event related spectral analysis. The power for each log scale frequency step was calculated from 3 to 45 Hz. These data were then time warped to a normalized gait cycle using the EEGLAB ERSP algorithm's built in time warp function. The gait events used to normalize were the lift of the left toe (LOFF, 0%), contact of the left heel (LON, 40%), lift of the right toe (ROFF, 50%), contact of the right heel (RON, 90%), and lift of the left toe again (LOFF, 100%) (Figure 2).

Spatial - Kinematics

Subjects' two-dimensional position in space was calculated using the projection of the primary head marker (front, center of head) down into the plane of the spiral (floor). The paths were further broken down into spatial segments by manual visual inspection of the path, marking where on the trajectory the point of the turn happened. This was necessary due to the unrestricted nature and therefore variability of the subjects' movement and path. In addition, an ID was assigned to each spatial segment, ID 1 being the longest, outermost segment, ID 2 the next longest at a 90 degree orientation to the first, and so on towards the center. The two dimensional trajectory was projected to a standardized straight line between the turn points allowing for the path to be normalized to a unit length. There are a total of 14 segments to the spiral, but due to the short length of the inner segments, the analysis was limited to only the longest 10 segments (ID 1-10).

Spatial - EEG

A custom preprocessing procedure, developed by our lab, was used to prepare the EEG data for space related analysis. Similar to the gait analysis, the data were first referenced to the average of the mastoid channels, high pass filtered at 1 Hz, and low pass filtered at 55 Hz. Events were created at every 1 second, continuously for the moving stretches (speed > 0.1 m/s). The data were then epoched from -500 ms to 500 ms around each walking event. This produced one-second epochs that were continuous in time. The data were then run through the same procedures of semi-automated and manual visual inspection of epochs for artifacts. ICA was run on the

resulting epochs and all artifactual ICs were removed from the data set. An average of 7.8 +/- 3.9 (mean +/- standard deviation) ICs were kept per each subject. The ICA weights were then applied on the continuous, non-epoched data, producing temporally continuous, clean data. The data were then subsequently filtered with a Kaiser window (www.scipy.org, width = 0.1/Nyquist, Nyquist = 512Hz, and ripple = 10dB) over multiple frequency ranges (1-4; 2-5Hz; 2-8Hz; 9-12Hz; 10-15Hz; 15-25Hz; 20-35Hz; 35-50Hz). A Hilbert transform was then applied to each frequency band, resulting in the instantaneous analytic amplitude, an analogue of power, as well as the phase.

RESULTS

Behavioral

Subjects each walked through the square spiral track at two different self-directed speeds. Each condition lasted for a total of ten minutes irrespective of individual variations in speed or path. Subjects were not forced to walk at a specific speed nor given feedback as to a target speed, and as such, there was variability in individual subjects' speeds. Figure 1b shows a sample subject's path with the instantaneous speed overlaid (colormap) for the 'slow' speed condition. Table 1 lists the speed and gait cycle values for all of the subjects. The first and third data columns detail the average speed and standard deviation of the distribution of speed values for each ten minute 'slow' and 'brisk' condition blocks, respectively. The mean of the individual average condition speeds were 0.65 +/- 0.15 m/s and 0.99 +/- 0.10 m/s for the 'slow' and 'brisk' speed, respectively. Paired t-test between the two conditions shows that the speed increased during the brisk condition, 0.3 +/- 0.1 (mean +/- 95% confidence) ($t(11)=7.68$, $p=1e-5$). Gait events were determined through visual inspection of the motion capture markers located on the feet of subjects. For subsequent gait event EEG analysis 'good' gait cycles were established in which all 5 necessary events were present and in correct order (LOFF, LON, ROFF, RON, LOFF; Figure 2A). These 'good' gait cycles were then tested for EEG artifacts, and any gait event that was determined to contain artifactual EEG was also removed. The resulting number of gait events used for the final EEG analysis is presented in table 1. Columns two and four contain the total amount of gait cycles that went into each individual

subject's analysis for the 'slow' and 'brisk' conditions, respectively. On the group scale, in the 'slow' speed condition, subjects had an average of 151 +/- 29 'good' gait cycles, and in the 'brisk' condition, subjects had an average 153 +/- 36 gait cycles. Paired t-test between number of good gate cycles shows no difference between the conditions ($t(11) = -0.276$, $p=0.78$).

Gait ERSP

The EEG, after being cleaned through statistical, manual, and ICA methods were back projected to the original electrode space. The data were then clustered into anatomically relevant groupings. Event related spectral perturbations (ERSP) were calculated locked to the onset of the gait cycle, then normalized to each of the gait events.

Figure 3 details the gait event related spectral characteristics of each subject (n=11; 1 subject was removed due to insufficient number of ICs) in both speed conditions and from the midline sensorimotor electrode cluster. The first column (Figure 3A) shows the unmasked, gait normalized ERSP for each subject in the 'slow' walking condition, baselined to the average power in each frequency range. The frequency ranges are plotted on a log scale. Positive power is indicated by the warmer colors and decreases in power by cooler colors. The power values range from -1.2 to 1.2 dB. From these plots we can begin to see structure in the activity. Most notably, we see changes in power that show up in a consistent manner with the progression the gait cycle. For example, Subject 5 (S5) shows cyclical changes in power in the low frequency range (3-5 Hz), initially decreasing in power for roughly the first 25% of the gait cycle, followed by an increase in power during the next 25% of the gait cycle.

This pattern of decrease then increase in power then repeats for the second half of the gait cycle. This results in a full two cycles of increase and decrease in power over the entire gait cycle. Similar patterns can be readily seen in some of the other subject's ERSPs (Figure 3A: S4, S5, S7, S8, and S10). Though there is clear consistency in some features, the overall ERSPs are considerably variable across subjects, as one would expect from an experiment that allows subjects to have the amount of freedom of action as this study does. Figure 3B details the decomposition of each subject's ERSP into single traces that are the average power over specific frequency ranges locked to the gait cycle (delta: 3-5 Hz, blue; theta: 5-8 Hz, red; alpha: 8-12 Hz, green; beta: 12-25 Hz, black). From the same subjects that showed cyclic activity in their ERSP, we can see the same pattern of activity in the single frequency band traces. Figure 3B, S5 delta (blue line) frequency demonstrates the full two cycles of consistent decreases then increases in power locked to the normalized gait cycle.

The third column (Figure 3C) details the same gait normalized ERSPs as in section A of the same figure but for the 'brisk' speed condition, baselined to the average power in each frequency band. The first observation is that there is a large amount of variability between conditions within the same subject. Most notably, within the 'brisk' condition there is a lack of the same cyclical activity in the delta frequency band. There are a couple of subjects that do show consistent low frequency cyclic activity (Figure 3C: S6 and S7) but the activity is both different from the features in the 'slow' condition and substantially different from each other within the same condition. Subjects' ERSPs in the 'brisk' speed condition do show consistent cyclic activity in the beta-band (12-25 Hz), and to a lesser degree, alpha-band (8-12

Hz) frequency range. Figure 3D, the mean activity in different frequency bands for the 'brisk' condition, shows this activity clearly. The beta traces (black) show the two cycle pattern of decreased then increased power over each half of the gait cycle in multiple subjects (Figure 3D: S2, S6, S8, S10).

Figure 4 depicts the average ERSPs for the 'slow' speed condition over the whole scalp, broken up into anatomically relevant clusters arranged parallel to the physical scalp layout. The bottom left figure depicts a top down view of the EEG electrode arrangements on the scalp. The highlighted electrodes are the ones used to average into clusters and the specific clusters are circled. The individual subject ERSP data were averaged across all the subjects (n=11) and plotted. The error across subjects was also calculated. From that, each point was determined to either be significant or not (95% confidence interval; $p<0.05$). Any values below that threshold were masked out to a value of 0 (green). The remaining significant points were plotted with their real power values, ranging from -0.5 to 0.5 dB for blue to red, respectively. The first main feature is the presence of statistically significant cyclical changes in power in the low frequency range (delta: 3-5 Hz). One complete cycle of decreased and increased power occurs during each half of the gait cycle, resulting in two full cycles for the length of the entire gait cycle. This observation is in the same manner as what was seen in individual subject (Figure 3A). Notably, the cyclic change in low frequency power only occurs significantly in the midline anterior clusters (midline sensorimotor and midline frontal, specifically). In addition, there is a large decrease in power that occurs at the right foot lift event (50% gait cycle). The effect is relatively widespread across electrode clusters, but is not uniform. It can be

seen that the strength and size of the decrease in power is larger in right hemisphere clusters, ipsilateral to the limb initiating movement, when compared to left hemisphere clusters, contralateral to limb movement.

For the 'brisk' speed condition the same average gait normalized ERSPs were calculated for each electrode cluster (Figure 5). The point by point variance across all subjects' ERSPs was calculated in the same way as in Figure 4. Additionally, all points below a 95% percent confidence rating ($p<0.05$) were again masked out in green (0 dB). The remaining data represents the average power across subjects of the particular frequency. Like the average ERSPs from the 'slow' speed condition, the more anterior clusters show statistically significance, but with cyclical changes in alpha- (8-12 Hz) and beta-band (12-25 Hz) power locked to the normalized gait cycle. Unlike the 'slow' speed condition, the effect is seen more widespread across hemispheres, specifically, the three frontal and three sensorimotor clusters as opposed to being localized to the midline. While the same two cycles of cyclic activity in the low frequencies is not seen during the 'brisk' condition, there is consistent significant decrease in power in the delta-/theta- band (3-8 Hz) during roughly the center of the swing phase of each leg. The decrease in power for the left leg swing phase (0-40% gait cycle) is much larger, more sustained, and over a wider frequency band than the corresponding activity in the right leg swing phase (50-90% gait cycle).

The power of specific frequency bands were separated for the midline frontal, left sensorimotor, right sensorimotor, and midline parietal clusters in the 'brisk' condition (Figure 6). The beta-band, and to a lesser degree, the alpha band show activity that strongly coincides with the normalized gait cycle. Having regions of

increased power and decreased power at the same intra-stride points of both legs. The other frequency bands do not show such a clean relation between power and percent along gait cycle.

Space

In addition to gait based analysis, each subjects' EEG were analyzed in reference to spatial location and navigation. The data were processed in a similar way as the gait analysis, though data from all the times in which a subject was walking (speed > 0.1 m/s) were used as opposed to just around the gait events. The data were cleaned with manual visual inspection and ICA decomposition. The resulting clean EEG data were back projected to the original electrode space. These data were then band pass filtered at relevant frequency bands (1-4, 2-5, 2-8, 9-13, 10-15, 15-25, 20-35, and 35-50 Hz). The analytic amplitude was calculated using the Hilbert transform on the band pass filtered data. This serves as an analogue to instantaneous power in the frequency band of interest. The analytic amplitudes were clustered into the same twelve regions as in the gait analysis, and then co-localized with each subject's path through the square spiral as calculated from their primary head marker.

The subjects' paths were then broken up into spatial segments (each straight side) of the square spiral. The path along the each segment was calculated by projecting the real location down to a linear normalized path from start to finish of each segment. These values were then divided by the real length producing a value for the progression along a normalized segment length (from 0 to 1). From previous work in our lab, activity in the high delta/theta band (2-8 Hz) recorded over midline

parietal cortex has shown to be related to spatial navigation (Snider et al., 2013). Figure 7 shows the analysis of the subjects' 2-8 Hz filtered analytic amplitude from the midline parietal cluster, plotted in reference to the normalized spatial segments. The first panel (Figure 7A) details the average amplitude of all the subjects (n=12) laid over the progression of each normalized spatial segment (10 segments total). The values are baselined to the mean of each segment. Red color represents a positive deviation from the mean activity and blue represents a decrease in activity. The color scale ranges from -1.4 to 1.4 microvolts. As can be seen, there are regions of increased amplitude consistently at specific locations along the normalized segment length across individual segments. Most notably, there is consistently increased EEG amplitude at roughly the 0.1-0.2 segment length location in multiple spatial segments (1, 2, 5, 6, 7, and 9).

Figure 7B presents the amplitude values averaged across all ten segments analyzed in Figure 7A. This plot demonstrates the activity that is consistent across all ten spatial segments. The dark blue line is the mean activity and the two light blue lines are the range indicating one standard deviation of the values across segments from the mean. Because this is relative power we can see points along the normalized segment that deviate substantially from the mean activity of the population (mean = 0). Such regions of activity are highlighted in gray. The most notable feature is the increase in amplitude at the same segment location noted above, roughly 0.1 to 0.2. The midline parietal electrode cluster signal appears to be increasing in amplitude within the 2-8 Hz range across all ten spiral segments at the same relative location.

This does not indicate a signal that is localizing with absolute space, but rather is a consistent signal at a specific relative spatial location.

Like the previous figure (Figure 7), Figure 8 shows the same analysis of 2-8 Hz filtered analytic amplitude of the midline parietal cluster in reference to the normalized spatial segments but from the 'slow' speed condition. The top panel (Figure 8A) shows definite structure across arms: consistent positivity near the beginning of many of the segments (1, 2, 3, 4, 8, and 10) and additional slight positivity at the end of almost all the segments. Figure 8B, shows the average of all the top panel's segments, giving a good representation of the overall analytic amplitude changes over the course of the normalized segment. The mean is indicated by the bold blue line and the standard deviation range is indicated by the two light blue lines. From these values, the regions highlighted in gray appear to be more positive than the mean activity across the segment. There is a region of increased activity at around the 0 to 0.1 segment length and at the end, 0.9 to 1.0 segment length. The most notable difference when compared to the 'brisk' speed condition results is the presence of another large area of increased activity at the end of the segments. Both conditions have a region of positive activity toward the start of the normalized segment.

DISCUSSION

To the best of our knowledge, this is the first experiment conducted on freely locomoting humans looking at gait cycle related cortical activity, and the first follow-up to previous work in our lab addressing the EEG of physical spatial navigation of humans. We aimed to address these topics by creating a paradigm in which EEG and full body motion capture were recorded while subjects simultaneously walk through open space in a square spiral track at two different speeds.

Gait events were obtained from inspection of the motion capture data from the markers located on each foot. Artifact rejected and ICA cleaned EEG data were co-localized to the gait events. The data were further clustered into anatomically relevant regions. Event related spectral perturbations (ERSP) were calculated and normalized to the gait events. From previously published treadmill walking experiments (Gwin et al., 2011) we hypothesized we would see spectral characteristics of EEG show cyclical changes in power in the alpha and beta bands (9-14 Hz and 14-25 Hz, respectively) coinciding with the swing phase of each leg, and theta-band (4-8 Hz) power decreasing during the swing phase of each leg and increasing during the stance phase, in which both feet were on the ground. Our results show that in the 'slow' speed condition, significant cyclical changes in low frequency (3-5Hz) power was observed in coordination with the normalized gait cycle. These findings were localized to the frontal and sensorimotor clusters along the midline. However, the decrease and increase of power both occurred within the swing phase, having no significant activity

during the dual stance phase. In addition, in the 'brisk' condition we see cyclical changes in power in the alpha (8-12Hz) and beta (12-25Hz) frequency bands coinciding mostly with the swing phases of each leg. Also, low frequency (3-8 Hz) decreases in power were seen during the swing phase, but no significance was seen during the stance phase. There were no significant findings in the low gamma (25-40 Hz) range in contrast with findings from robot orthosis assisted gait (Seeber et al., 2014). While some of the details are different these findings are similar enough to the existing literature that they serve as support for specific EEG characteristics that are present during human gait.

The alpha and beta band findings could be explained by motor control requirements involved in locomotion. It has been shown that alpha and beta power decrease in response to lower limb motor control (Wieser et al. 2010, Heidemann et al. 2014). The motor movements involved in gait are not discrete but rather continuous and cyclical. As such, a signal indexing cortical control of the lower limb muscles would presumably also be cyclical. In the case of our results, there is decreasing power in alpha/beta range to the initial leg push off and movement, then an increase in power during the sustained swing phase, followed by alpha/beta power decreases at the other leg's push off. This cyclic modulation of power in the alpha/beta frequency bands then repeats. Decrease in beta power over sensorimotor areas has been shown to correlate with the initiation of new actions (Meirovitch et al., 2015; Nakayashiki et al., 2014). In addition, increase in beta has been attributed to maintaining the current motor state (Solis-Escalante et al., 2012; Sallard et al., 2014). During natural gait, one would expect a decrease in beta around the push off/initiation of the swing phase of

one leg's movement. Following this, an increase in beta while the swing was maintained would coincide appropriately with the fact that cortex need not exhibit as much top down control, relying more on the leg's biomechanical properties. The lack of significant cyclical beta power in the 'slow' condition could be explained by the difference in biomechanical requirements to walk at such a slow pace (0.65 m/s). In addition, changes in beta power before and during reaching movements are different for different peak speeds, enough to reasonably classify the movements from EEG alone (Yang et al. 2015). Presumably, the same modulation in cortical involvement applies to the lower limb control involved in slow speed gait.

Though Gwin and colleagues (2011) mentioned they found no significant differences in the spectral characteristics of EEG for their two speeds, 0.8 m/s and 1.2 m/s, it has been shown variable speed in treadmill walking does have an effect on scalp EEG (Bulea et al., 2015). Our results indicate a substantial difference in the frequency characteristics of EEG between the two conditions. During the 'slow' and 'brisk' condition, subjects walked at an average speed of 0.65 m/s and 0.99 m/s, respectively. In addition, our experiment, by design forces subjects to modulate their speed and gait in response to the spiral track. As such, the difference in event related spectral results may be due to the variability in gait and speed parameters within our experiment. An experiment that could be used to test whether variability in walking mechanics alone would cause the difference, would be to design an paradigm in which subjects walk on a linear track at multiple speeds and for different lengths.

These findings serve as an initial exploration into the topic of complex motor control of humans in naturalistic paradigms and environments. Further implications of

this research could be to objectively analyze the electrocortical effects certain diseases have on brain dynamics of motor control, such as Parkinson's disease.

In animal models, it has been shown that single cells within the parietal cortex respond to aspects of a spatial route in a repeatable manner (Nitz, 2006; Nitz, 2012). Previous work from our lab has implicated EEG signals from parietal electrodes being correlated with the subject's spatial location (Snider et al., 2013) in a similarly physically unrestricted paradigm. Furthermore, preliminary work in the same experimental paradigm has shown that the power in low-theta (2-5 Hz) frequencies co-localizes with the relative location in a spatial route (Trees et al., 2013). We predicted that we would similarly find theta range activity to be locked to space. We found that the analytic amplitude (analogue of instantaneous power) of 2-8Hz filtered EEG from the midline parietal cluster showed substantial spatial regularity in power along a relative path. There appears to be a consistent pattern of low frequency power changes along a normalized segment of the square spiral irrespective of direction, orientation, or length. At a 'brisk' speed, there was a consistent increase in power towards the beginning of each segment, whereas at the 'slow' speed there were both consistent activity at the beginning and at the end of all the segments. While this signal does not index a subject's absolute location, it is another finding of a spatial navigation related signal in humans physically navigating space. A proposed follow up experiment would be to have subjects walk back and forth along a single linear path, of which the length could be changed by using a virtual environment. This would restrict the subject to two directions and a single segment orientation, allowing for a finer resolution of control on the intended path.

Study of physical human spatial navigation is still vastly underserved. This experiment aims help fill the gap in our direct empirical understanding of how we navigate our environment. It is well documented that diseases like Alzheimer's have indicated relatively early by deficits in spatial navigation (Tangen et al., 2015). Understanding the neural correlates navigation in healthy individuals could lead to a better understanding of the differences in diseased populations. This could ultimately lead to early detection of these diseases, even before symptoms appear.

TABLES

Table 1: Behavioral measures. Included are the average speeds traveled of each subject in each condition along with the number of 'good' gait cycles used in subsequent analysis. Paired t-test between number of good gate cycles shows no difference between the conditions ($t(11) = -0.276$, $p=0.78$). Paired t-test between the two conditions shows that the speed increased during the brisk condition (0.3 +/- 0.1 (mean +/- 95% confidence) $t(11)=7.68$, $p=1e-5$).

	Slow		**Brisk**	
Subject	**Speed (m/s)**	**# gait cycles**	**Speed (m/s)**	**# gait cycles**
1	0.52 +/- 0.22	167	1.13 +/- 0.33	164
2	0.45 +/- 0.13	148	0.97 +/- 0.24	191
3	0.69 +/- 0.24	123	0.90 +/- 0.27	145
4	0.63 +/- 0.14	186	0.99 +/- 0.25	220
5	0.95 +/- 0.19	200	1.23 +/- 0.40	167
6	0.56 +/- 0.22	131	1.07 +/- 0.35	133
7	0.82 +/- 0.32	113	0.91 +/- 0.51	78
8	0.60 +/- 0.16	170	0.96 +/- 0.23	175
9	0.75 +/- 0.17	166	0.99 +/- 0.28	183
10	0.53 +/- 0.15	95	0.88 +/- 0.30	114
11	0.79 +/- 0.15	164	0.96 +/- 0.22	140
12	0.49 +/- 0.12	157	0.92 +/- 0.20	135

FIGURES

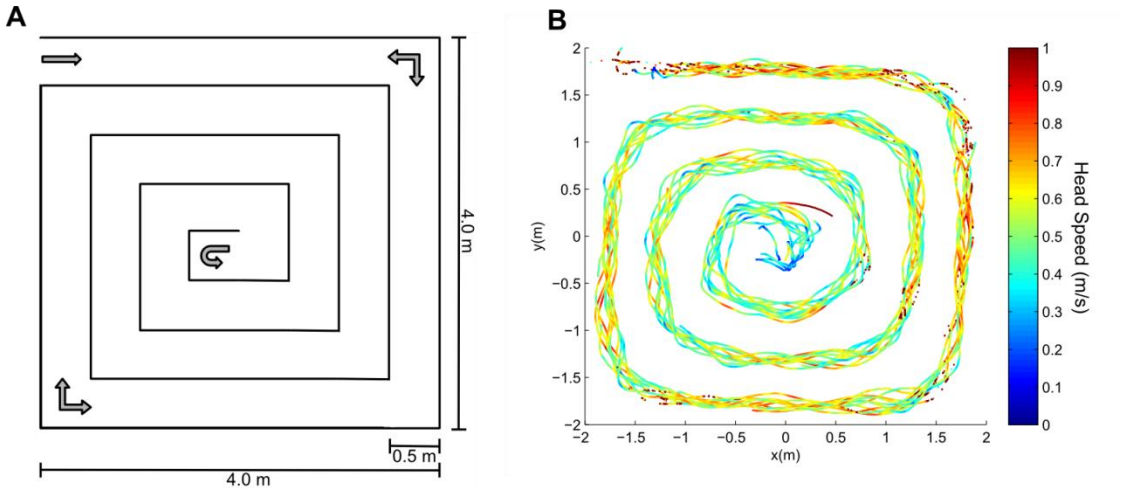

Figure 1: Square spiral track and example path. **A** Schematic of the 4m x 4m square spiral track. Tape was used to mark the spiral's boundaries on the floor of the experimental space. Subjects move from the outermost segment towards the center, turn around, move towards the start, and repeat for a total of ten minutes. **B** Example of a single subject's raw head trajectory (10 min. of data) from the "comfortable walk" condition projected onto the square spiral. The colormap represents the instantaneous speed of the same head marker.

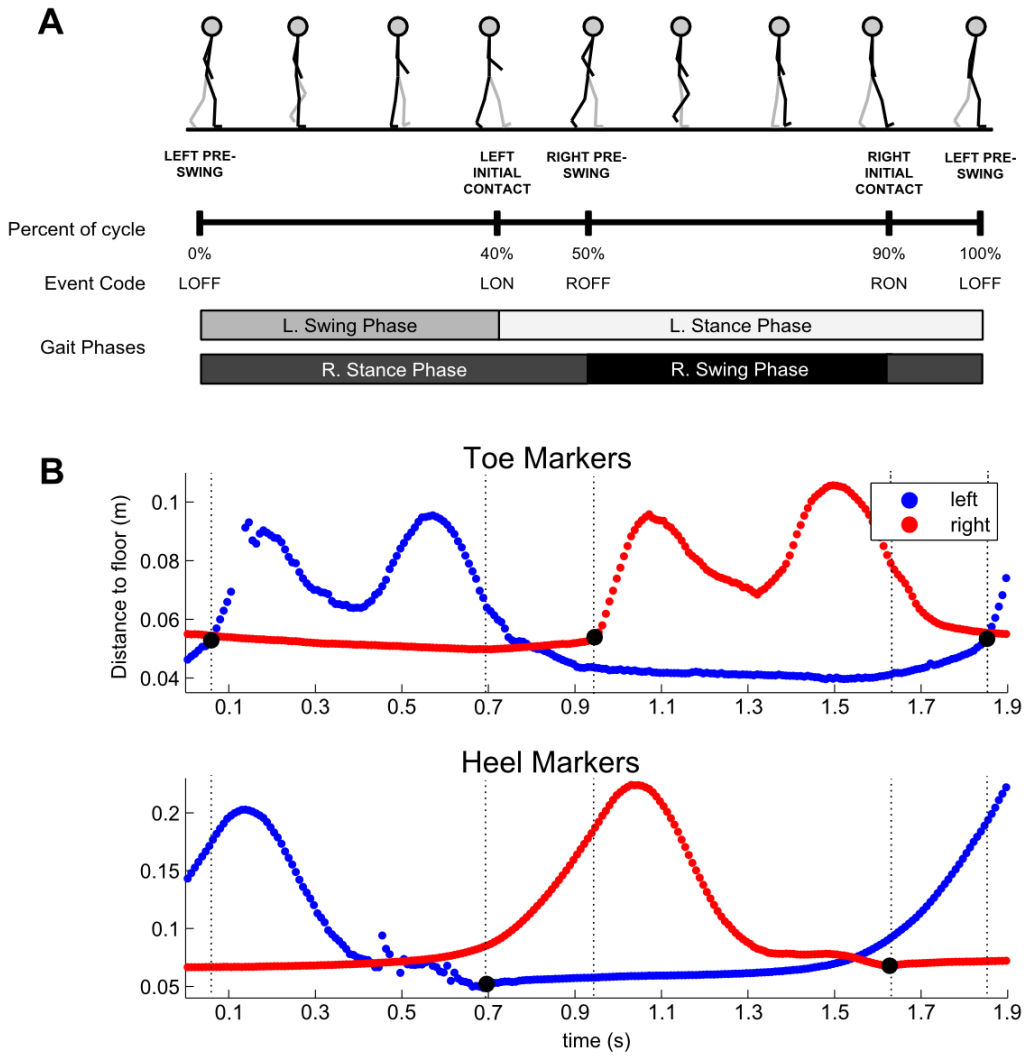

Figure 2: Gait cycle phases and events. **A** Gait cycle breakdown. Top, Illustration representing a subject's gait. Middle, graph detailing the 5 relevant events (LOFF, LON, ROFF, RON, and LOFF) used in subsequent normalized analyses along with the corresponding assigned percentage of gait cycle. Bottom, Graphical representation of each leg's independent gait cycle phases. **B** Gait event interface. Top, the vertical displacement of the left and right foot's toe markers over time. Black dots with dotted lines mark the relevant events of the gait cycle on the raw data. Bottom, vertical displacement of the corresponding foot's heel markers. Events were assigned by visual inspection of the vertical displacement graphs and were confirmed with 3D point reconstruction of the foot marker trajectory.

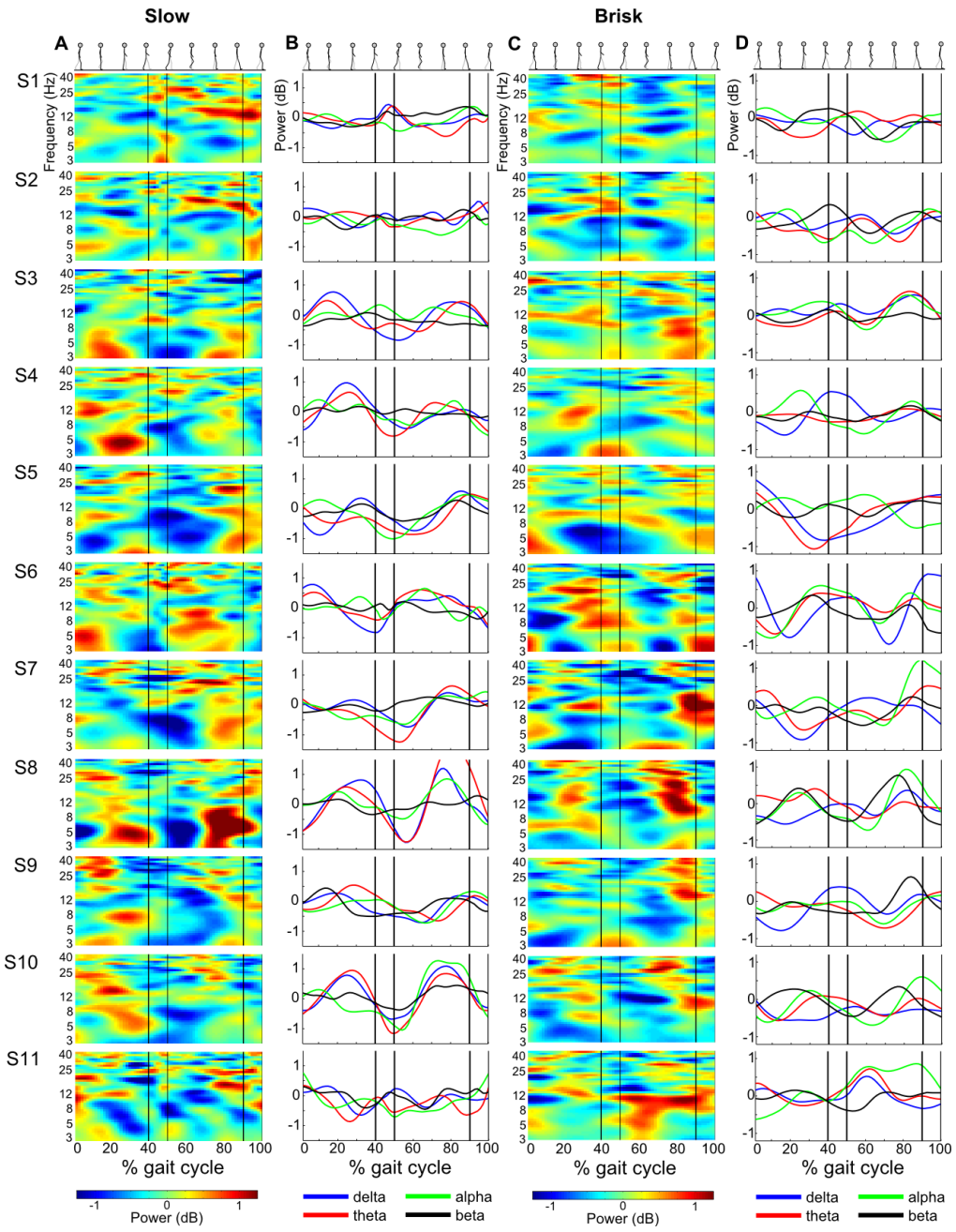

Figure 3: ERSP of each subject in each condition. **A** Time normalized ERSPs of individual subjects in the "comfortable speed" condition. Vertical black lines represent the relevant events and the points at which the data is normalized to. Frequencies are plotted in log spacing with increase and decrease in power represented by red and blue, respectively. **B** ERSP results broken down into traces for the average activity in the given frequency bands over the normalized gait cycle (delta: 3-5Hz, theta: 5-8Hz, alpha: 8-12 Hz, beta: 12-25). **C**,**D** The same results as **A** and **B**, respectively, but for the "brisk speed" condition.

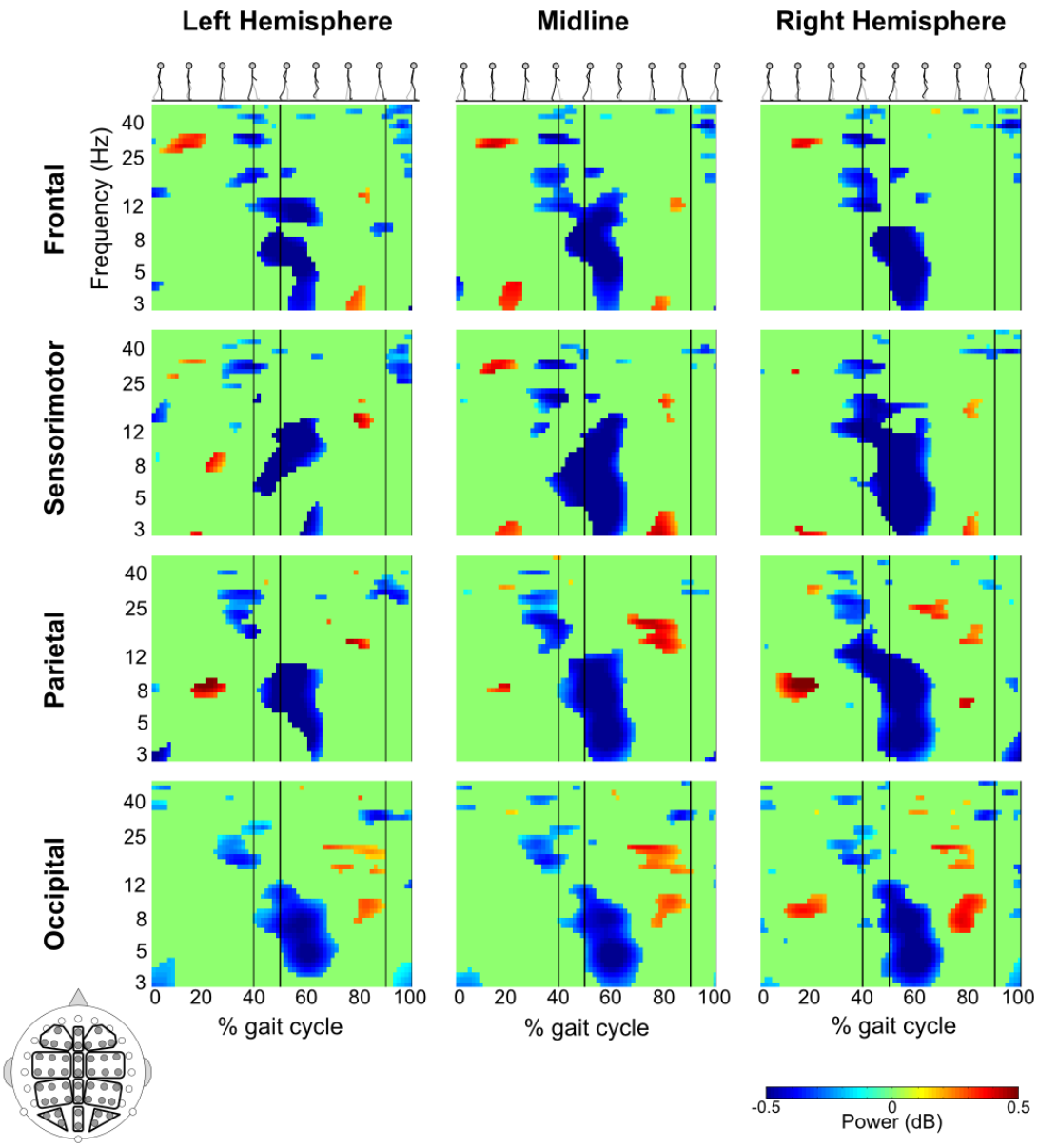

Figure 4: All clusters average ERSPs for 'slow' speed. Results for the average gait normalized ERSP across all subjects from each electrode cluster in the 'slow' speed condition. The plots show significant regions of activity that are consistent across the subject population. The data are masked at a 95% confidence interval across all subjects ($p<0.5$). Bottom-left, figure showing the electrodes that were averaged for each cluster above.

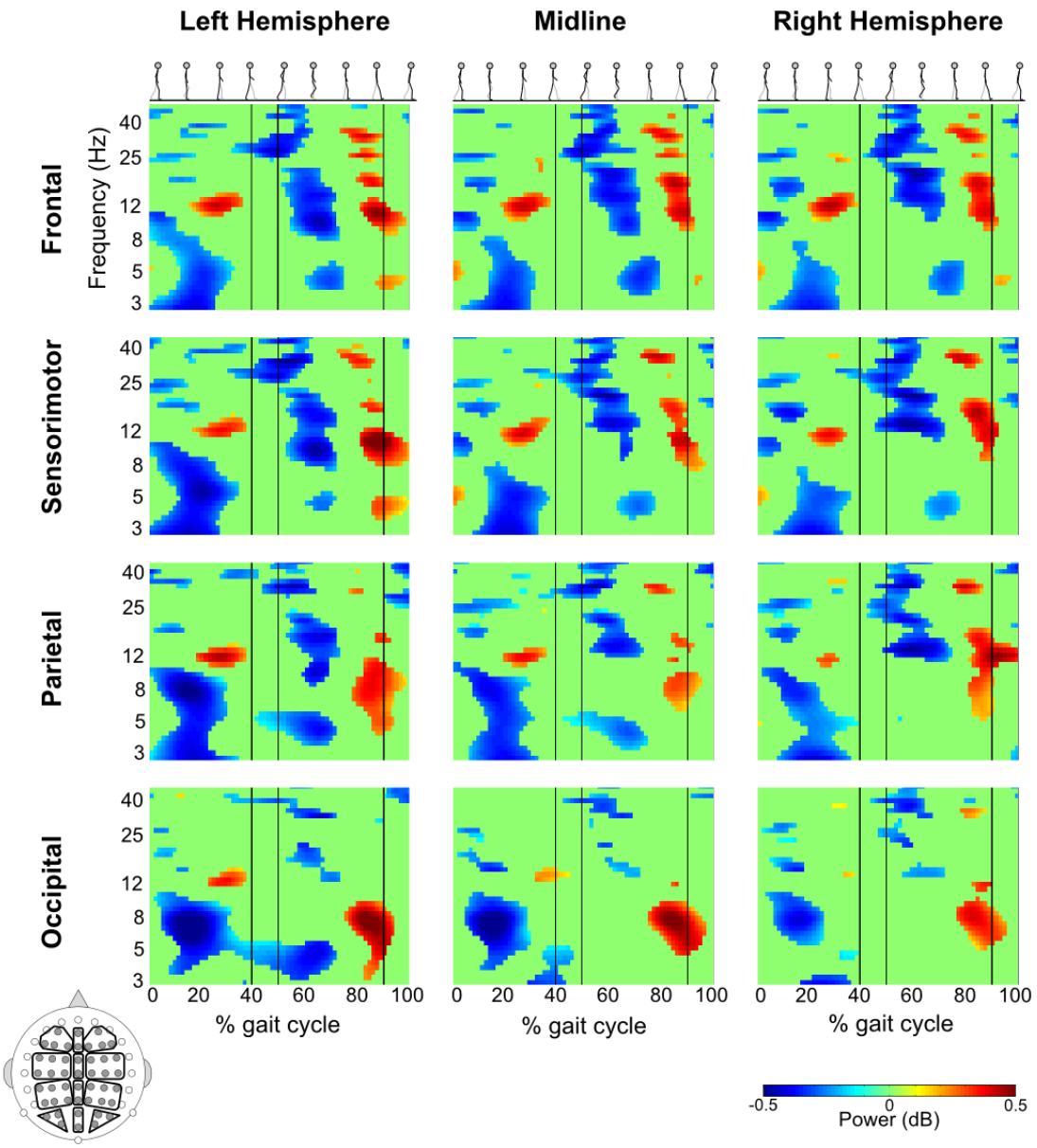

Figure 5: All clusters average ERSPs for 'brisk' speed. Results for the average gait normalized ERSP across all subjects from each electrode cluster in the 'brisk' speed condition. The plots show significant regions of activity that are consistent across the subject population. The data are masked at a 95% confidence interval across all subjects ($p<0.5$). Bottom-left, figure showing the electrodes that were averaged for each cluster above.

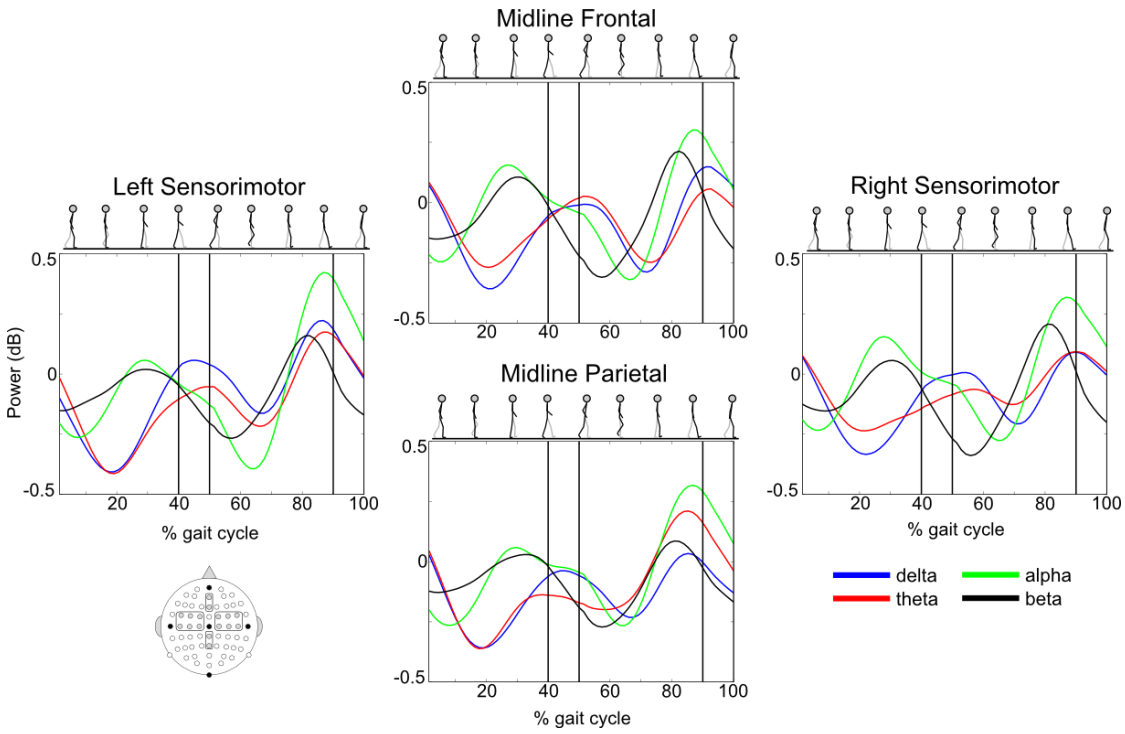

Figure 6: Frequency band traces over midline and sensorimotor clusters. Changes in power of specific frequency bands normalized to the gait cycle. The data are the average power in each of the frequency bands for the "brisk speed" condition (delta: 3-5Hz, theta: 5-8Hz, alpha: 8-12 Hz, beta: 12-25). Bottom right, figure shows the electrodes contributing to each cluster. The beta frequency range (black), in particular, shows consistent changes in spectral power coinciding with the normalized gait cycle.

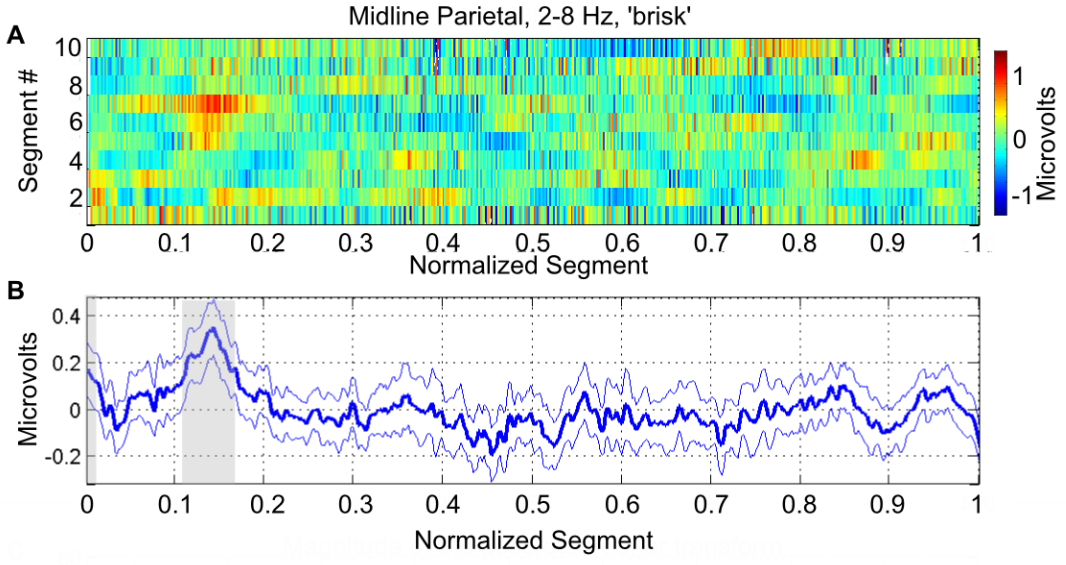

Figure 7: Parietal cluster theta activity over normalized spatial segments in the 'brisk' speed condition. Analytic amplitude of 2-8 Hz filtered EEG from the midline parietal cluster. **A** The analytic amplitude averaged across subjects for each of the spatial segments (1-10) locked to the progression along each normalized segment. Values are baselined to the mean of each segment, with positive values plotted in red and negative in blue. **B** The overall mean activity across segments, from the across subject activity in (A). Error range is one standard deviation of the across arms distribution. Regions that deviate significantly from zero are highlighted in gray.

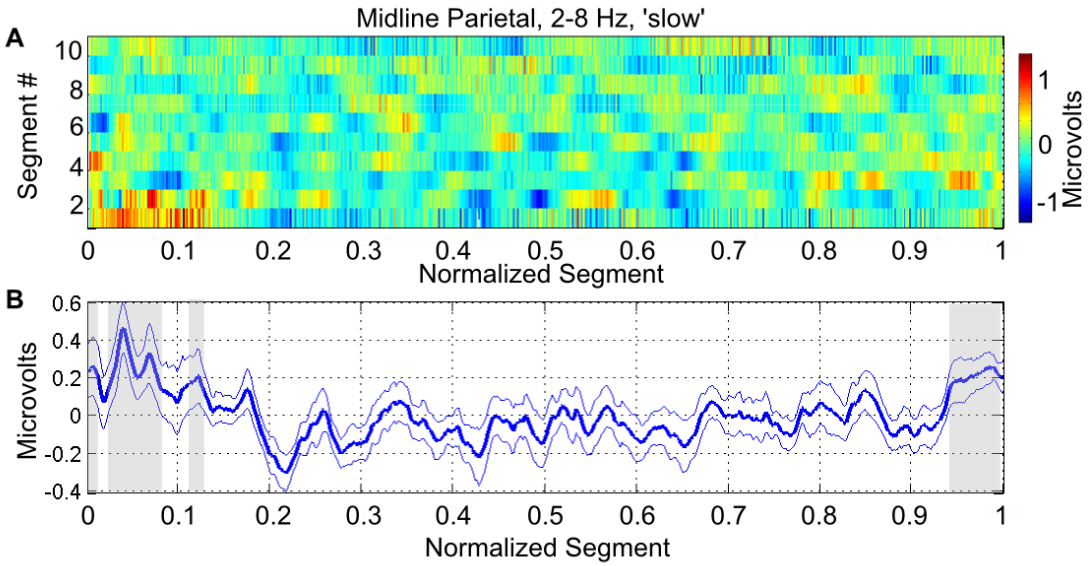

Figure 8: Parietal cluster theta activity over normalized spatial segments in the 'slow' speed condition. Analytic amplitude of 2-8 Hz filtered EEG from the midline parietal cluster. **A** The analytic amplitude averaged across subjects for each of the spatial segments (1-10) locked to the progression along each normalized segment. Values are baselined to the mean of each segment, with positive values plotted in red and negative in blue. **B** The overall mean activity across segments, from the across subject activity in (A). Error range is one standard deviation of the across arms distribution. Regions that deviate significantly from zero are highlighted in gray.

REFERENCES

Andersen RA (1995) Encoding of intention and spatial location in the pos- terior parietal cortex. Cereb Cortex 5:457– 469.

Aronov D, Tank DW. Engagement of neural circuits underlying 2D spatial navigation in a rodent virtual reality system. Neuron. 2014 Oct 22;84(2):442-56

Bell AJ, Sejnowski TJ. Learning the higher-order structure of a natural sound. Network. 1996 May;7(2):261-7.

Bulea TC, Kim J, Damiano DL, Stanley CJ, Park HS. Prefrontal, posterior parietal and sensorimotor network activity underlying speed control during walking. Front Hum Neurosci. 2015;9:247.

Burgess N, O'Keefe J (2011) Models of place and grid cell firing and theta rhythmicity. Curr. Opin. Neurobiol. 21, 734–744

Buzsáki G, Moser EI (2013) Memory, navigation and theta rhythm in the hippocampal-entorhinal system. Nature Neuroscience. 16(2):130-8.

Cabral HO, Fouquet C, Rondi-Reig L, Pennartz CM, Battaglia FP. Single-trial properties of place cells in control and CA1 NMDA receptor subunit 1-KO mice. J Neurosci. 2014 Nov 26;34(48):15861-9

Clower DM, West RA, Lynch JC, Strick PL (2001) The inferior parietal lob- ule is the target of output from the superior colliculus, hippocampus, and cerebellum. J Neurosci 21:6283– 6291. Medline

Cimolin V, Galli M. Summary measures for clinical gait analysis: a literature review. Gait Posture. 2014 Apr;39(4):1005-10

Derdikman D, Moser EI. (2010) A Manifold of spatial maps in the brain. Trends Cogn. Sci. 14, 561-569.

Delorme A, Makeig S. EEGLAB: an open source toolbox for analysis of single-trial EEG dynamics including independent component analysis. J Neurosci Methods. 2004 Mar 15;134(1):9-21.

Delval A, Tard C, Defebvre L. Why we should study gait initiation in Parkinson's disease. Neurophysiol Clin. 2014 Jan;44(1):69-76.

Doeller CF, Barry C, Burgess N (2010) Evidence for grid cells in a human memory network. Nature 463, 657–661

Etienne S, Guthrie M, Goillandeau M, Nguyen TH, Orignac H, Gross C, Boraud T. Easy rider: monkeys learn to drive a wheelchair to navigate through a complex maze. PLoS One. 2014;9(5):e96275

Furuya Y, Matsumoto J, Hori E, Boas CV, Tran AH, Shimada Y, Ono T, Nishijo H. Place-related neuronal activity in the monkey parahippocampal gyrus and hippocampal formation during virtual navigation. Hippocampus. 2014 Jan;24(1):113-30

Fyhn M, Hafting T, Treves A, Moser MB, Moser EI (2007) Hippocampal remapping and grid realignment in entorhinal cortex. Nature 446, 190–194

Geva-Sagiv M, Las L, Yovel Y, Ulanovsky N. Spatial cognition in bats and rats: from sensory acquisition to multiscale maps and navigation. Nat Rev Neurosci. 2015 Feb;16(2):94-108

Gwin JT, Gramann K, Makeig S, Ferris DP. Electrocortical activity is coupled to gait cycle phase during treadmill walking. Neuroimage. 2011 Jan 15;54(2):1289-96

Hafting T, Fyhn M, Molden S, Moser MB, Moser EI (2005) Microstructure of a spatial map in the entorhinal cortex. Nature 436 (7052): 801–806.

Heideman SG, te Woerd ES, Praamstra P. Rhythmic entrainment of slow brain activity preceding leg movements. Clin Neurophysiol. 2015 Feb;126(2):348-55

Hsu YL, Chung PC, Wang WH, Pai MC, Wang CY, Lin CW, Wu HL, Wang JS. Gait and balance analysis for patients with Alzheimer's disease using an inertial-sensor-based wearable instrument. IEEE J Biomed Health Inform. 2014 Nov;18(6):1822-30

Leutgeb S, Mizumori SJ (1999) Excitotoxic septal lesions result in spatial memory deficits and altered flexibility of hippocampal single-unit representations. J Neurosci. 19(15):6661-72.

Lithfous S, Dufour A, Després O. Spatial navigation in normal aging and the prodromal stage of Alzheimer's disease: insights from imaging and behavioral studies. Ageing Res Rev. 2013 Jan;12(1):201-13

McNaughton BL, Battaglia FP, Jensen O, Moser EI, & Moser MB (2006) Path integration and the neural basis of the ‘cognitive map’. Nat. Rev. Neurosci. 7, 663–678

Meirovitch Y, Harris H, Dayan E, Arieli A, Flash T. Alpha and beta band event-related desynchronization reflects kinematic regularities. J Neurosci. 2015 Jan 28;35(4):1627-3

Muller RU and Kubie JL (1987) The effects of changes in the environment on the spatial firing of hippocampal complex-spike cells. J. Neurosci. 7, 1951–1968

Nakayashiki K, Saeki M, Takata Y, Hayashi Y, Kondo T. Modulation of event-related desynchronization during kinematic and kinetic hand movements. J Neuroeng Rehabil. 2014 May 30;11:90

Nitz DA (2006) Tracking route progression in the posterior parietal cortex. Neuron, 49: 747-756.

Nitz DA (2012) Spaces within spaces: rat parietal cortex neurons register position across three reference frames. Nat Neurosci. 215(10):1365-7

O'Keefe J. (1976). Place units in the hippocampus of the freely moving rat. Exp. Neurol. 51, 78–109.10.1016/0014-4886(76)90055-8
Olton DS, Samuelson RJ (1976) Remembrance of places passed: spatial memory in rats. J. Exp. Psychol. [Anim. Behav.]. 2:97-116

Petersen CC. Cortical control of whisker movement. Annu Rev Neurosci. 2014;37:183-203

Richard GR, Titiz A, Tyler A, Holmes GL, Scott RC, Lenck-Santini PP. Speed modulation of hippocampal theta frequency correlates with spatial memory performance. Hippocampus. 2013 Dec;23(12):1269-79

Sallard E, Tallet J, Thut G, Deiber MP, Barral J. Post-switching beta synchronization reveals concomitant sensory reafferences and active inhibition processes. Behav Brain Res. 2014 Sep 1;271:365-73

Seeber M, Scherer R, Wagner J, Solis-Escalante T, Müller-Putz GR. EEG beta suppression and low gamma modulation are different elements of human upright walking. Front Hum Neurosci. 2014;8:485

Solis-Escalante T, Müller-Putz GR, Pfurtscheller G, Neuper C. Cue-induced beta rebound during withholding of overt and covert foot movement. Clin Neurophysiol. 2012 Jun;123(6):1182-90

Snider J, Plank M, Lynch G, Halgren E, Poizner H. (2013) Human cortical θ during free exploration encodes space and predicts subsequent memory. J Neurosci. 33(38):15056-68.

Snider J, Plank M, Lee D, Poizner H. Simultaneous neural and movement recording in large-scale immersive virtual environments. IEEE Trans Biomed Circuits Syst. 2013 Oct;7(5):713-21

Svoboda J, Telensky P, Blahna K, Vodicka M, Stuchlik A. The role of rat posterior parietal cortex in coordinating spatial representations during place avoidance in dissociated reference frames on a continuously rotating arena (Carousel). Behav Brain Res. 2015 May 16

Tangen GG, Engedal K, Bergland A, Moger TA, Hansson O, Mengshoel AM. Spatial navigation measured by the Floor Maze Test in patients with subjective cognitive impairment, mild cognitive impairment, and mild Alzheimer's disease. Int Psychogeriatr. 2015 Feb 3:1-9

Terrazas A, Krause M, Lipa P, Gothard KM, Barnes CA, McNaughton BL (2005) Self-motion and the hippocampal spatial metric. J Neurosci 25: 8085– 8096.1

Trees J, Snider J, Halgren E, Poizner H. Human electrocortical dynamics of spatial navigation ina predefined square spiral. Neural Engineerng, 2013 6th International IEEE/EMBS Conference Preceedings

Vorhees CV, Williams MT. Assessing spatial learning and memory in rodents. ILAR J. 2014;55(2):310-32

Watrous AJ, Lee DJ, Izadi A, Gurkoff GG, Shahlaie K, Ekstrom AD. A comparative study of human and rat hippocampal low-frequency oscillations during spatial navigation. Hippocampus. 2013 Aug;23(8):656-61

Wills TJ, Muessig L, Cacucci F. The development of spatial behaviour and the hippocampal neural representation of space. Philos Trans R Soc Lond B Biol Sci. 2013 Dec 23;369(1635):20130409.

Wolbers T, Wiener JM. Challenges for identifying the neural mechanisms that support spatial navigation: the impact of spatial scale. Front Hum Neurosci. 2014;8:571.

Yang L, Leung H, Plank M, Snider J, Poizner H. EEG activity during movement planning encodes upcoming peak speed and acceleration and improves the accuracy in predicting hand kinematics. IEEE J Biomed Health Inform. 2015 Jan;19(1):22-8.

Zarka D, Cevallos C, Petieau M, Hoellinger T, Dan B, Cheron G. Neural rhythmic symphony of human walking observation: Upside-down and Uncoordinated condition on cortical theta, alpha, beta and gamma oscillations. Front Syst Neurosci. 2014;8:169